PHOTONICS Research

# On-chip integrated few-mode erbium–ytterbium co-doped waveguide amplifiers

Xiwen He,[1,2,†] Deyue Ma,[1,2,†] Chen Zhou,[1,3] Mingyue Xiao,[4] Weibiao Chen,[1,2] and Zhiping Zhou[1,5,*]

[1]Aerospace Laser Technology and Systems Department, Shanghai Institute of Optics and Fine Mechanics, Chinese Academy of Sciences, Shanghai 201800, China
[2]Center of Materials Science and Optoelectronics Engineering, University of Chinese Academy of Sciences, Beijing 100049, China
[3]School of Physical Sciences, University of Science and Technology of China, Hefei 230026, China
[4]School of Microelectronics, Shanghai University, Shanghai 201800, China
[5]State Key Laboratory of Advanced Optical Communications Systems and Networks, School of Electronics, Peking University, Beijing 100871, China
[†]These authors contributed equally to this work.
*Corresponding author: zjzhou@pku.edu.cn

Received 20 December 2023; revised 28 February 2024; accepted 5 March 2024; posted 7 March 2024 (Doc. ID 516242); published 1 May 2024

**We propose for the first time, to the best of our knowledge, an on-chip integrated few-mode erbium–ytterbium co-doped waveguide amplifier based on an 800 nm thick $Si_3N_4$ platform, which demonstrates high amplification gains and low differential modal gains (DMGs) simultaneously. An eccentric waveguide structure and a co-propagating pumping scheme are adopted to balance the gain of each mode. A hybrid mode/polarization/wavelength-division (de)multiplexer with low insertion loss and crosstalk is used for multiplexing and demultiplexing in two operation wavebands centered at 1550 nm and 980 nm, where the light in these two bands serves as the signal light and pump light of the amplifier, respectively. The results demonstrate that with an input signal power of 0.1 mW, $TE_0$ mode pump power of 300 mW, and $TE_1$ mode pump power of 500 mW, the three signal modes ($TE_0/TM_0/TE_1$) all exhibit amplification gains exceeding 30 dB, while maintaining a DMG of less than 0.1 dB.** 

https://doi.org/10.1364/PRJ.516242

## 1. INTRODUCTION

In the information age, with the explosive growth of data, the transmission capacity of single-mode fiber (SMF) optical communication systems has approached the Shannon limit [1], making it difficult to carry more digital information. In order to overcome this capacity crunch and further improve the transmission capacity of SMF, it is proposed to expand the spatial dimension of optical fibers using methods such as wavelength-division multiplexing (WDM) [2], time-division multiplexing (TDM) [3], and space-division multiplexing (SDM) [4]. Mode-division multiplexing (MDM) technology based on few-mode fiber (FMF) is the most important type of SDM technology [5–10]. Different modes in FMF are orthogonal to each other and can be used as independent channels for data transmission, thus significantly improving the transmission capacity of SMF. Currently, the development of MDM technology has made some progress; some key devices have been developed, such as mode (de)multiplexers [11–13], mode converters [14–16], and mode filters [17,18]. During long-distance transmission, due to fiber transmission losses, in order to ensure the signal quality at the receiving end, it is often necessary to use erbium-doped fiber amplifiers (EDFAs) to amplify the optical signal and compensate for the loss. A traditional SM-EDFA cannot amplify each mode in FMF, so it is essential to study an FM-EDFA suitable for amplifying different mode signals [19,20].

Compared with EDFAs, erbium-doped waveguide amplifiers (EDWAs) offer several advantages. First, they eliminate the need for several meters of erbium-doped fiber for amplification. This not only simplifies the setup but also allows for higher net gain within a smaller device size [21–24]. Moreover, EDWAs boast a higher integration level, enabling heterogeneous integration with various active and passive optical devices on the same chip [25–27]. These devices include modulators, photodetectors, waveguide couplers, waveguide filters, etc. While single-mode erbium-doped waveguide amplifiers (SM-EDWAs) have attracted significant research attention, there has been limited exploration of FM-EDWA [28–30]. This is mostly because the few-mode waveguide amplifier has to overcome two significant obstacles. The first is that each mode's amplification effect must be maximized to the fullest extent possible. The second is that the differential

modal gain (DMG) must be addressed, as too much DMG can negatively affect the few-mode amplifier's overall performance and impair normal operation.

To enhance the net gain of waveguide amplifiers within limited chip area, current approaches primarily concentrate on lowering waveguide losses, minimizing gain saturation effects, and raising the effective erbium doping concentration. Ligentec's 800 nm thick $Si_3N_4$ waveguides [31,32] are well-suited for high-power amplification because of their ultra-low transmission losses (<5 dB/m) and ability to handle continuous high-power laser input without causing damage to the waveguide. Furthermore, a greater percentage of the optical field is confined within the waveguide region of thick $Si_3N_4$ waveguides, which makes it easier to achieve higher net gains. The erbium–ytterbium (Er-Yb) co-doping approach is used to decrease gain saturation and improve effective doping concentration [33–37]. Using this technique, ytterbium ions are added to the erbium-doped material system as sensitizers and diluents. This results in a highly effective sensitization effect by allowing ytterbium ions to absorb more energy from the 980 nm pump light and transmit it to erbium ions.

It is essentially best to have similar overlap factors for different modes of light in the doping region as much as feasible in order to reduce DMG and achieve gain balance among different modes. Currently, there are two primary approaches for gain equalization: using a pumping technique that combines many pump light modes, or improving the doping distribution of erbium ions in few-mode waveguides [28,29]. By utilizing the advantages of polymer processing, Zhang *et al.* suggested a core doping arrangement to maximize the doping distribution of erbium ions in few-mode waveguides [28]. Layered doping is used in the design of the optical waveguide, with high doping concentration in the outside layer and low doping concentration in the core layer. The goal of this design is to lower DMG and balance the signal light fields of the various modes. With layered doping and genetic algorithm optimization, they were able to obtain a gain of about 22 dB and DMG <0.5 dB for the five-mode group few-mode erbium–ytterbium co-doped waveguide amplifier (FM-EYCDWA). However, on-chip integrated FM-EYCDWA implementation based on this doping technique is still difficult and complex. Another strategy is to introduce high-order or combination mode pump light into a few-mode waveguide in order to optimize the pumping scheme. In 2021, Yu and colleagues utilized a genetic algorithm to optimize the power distribution of several pump lights, resulting in an average gain of 10.4 dB and DMG <0.4 dB when using the combined pump of $LP_{01}$ and $LP_{21b}$ [29]. Although this approach is easier to implement, the fundamental mode signal may lose a large amount of gain in order to balance the DMG.

In this paper, we propose a method to solve the trade-off between high net gains of each mode and DMGs in on-chip FM-EYCDWA by using an eccentric waveguide structure with a co-propagating pumping scheme. Moreover, due to the novel design of a hybrid mode/polarization/wavelength-division (de) multiplexer, which combines various modes of signal light and pump light, we no longer need to use off-chip mode-selective photonic lanterns for mode multiplexing and demultiplexing. The results demonstrate that the FM-EYCDWA supports the even amplification of three signal modes ($TE_0$, $TM_0$, and $TE_1$), and the gains of all the three modes exceed 30 dB, with a DMG of less than 0.1 dB. Benefiting from this design, we can change the eccentric structure to directly manipulate the distribution of various modes in the Er-Yb co-doped region, thereby improving the gain equalization effects between different signal modes. This method is easy to implement in terms of process and is expected to support more modes in the future.

## 2. DESIGN OF FM-EYCDWA

The FM-EYCDWA is designed on an 800 nm thick $Si_3N_4$ platform. A two-dimensional (2D) schematic diagram of the on-chip FM-EYCDWA is displayed in Fig. 1; it can be observed that the chip consists of three regions: two passive areas and one active area. The passive region serves as a wavelength, mode, and polarization (de)multiplexer, while the active region contains an Er-Yb co-doped few-mode waveguide. At the input end, the MUX receives $TE_0$ mode light at 1550 nm and 980 nm, and after mode and polarization conversion, it couples the light into a few-mode bus waveguide. In the FM waveguide, there are simultaneously modes including 1550 nm $TE_0$, $TE_1$, and $TM_0$, and 980 nm $TE_0$ and $TE_1$. The refractive index of the erbium–ytterbium co-doped material (1.97 at 1.55 μm) is similar to that of $Si_3N_4$ (2.0 at 1.55 μm), resulting in a comparable mode field distribution in waveguides of the same thickness. To address the DMG problem

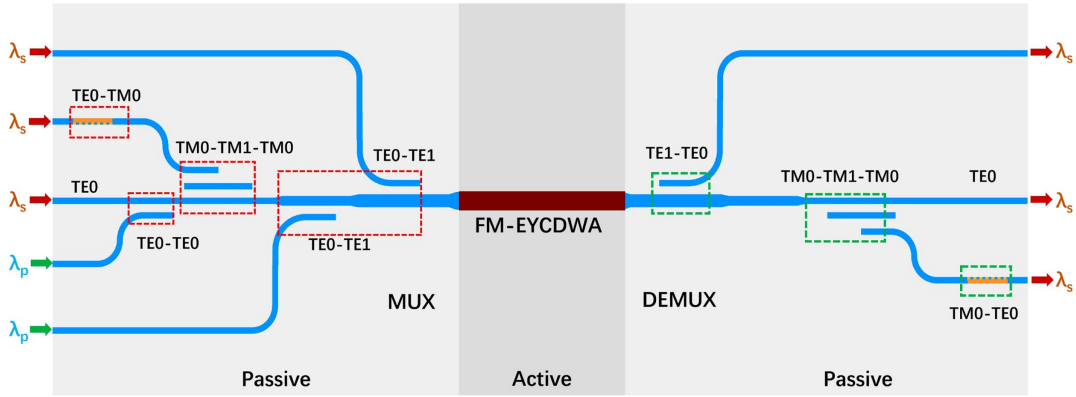


**Fig. 1.** Schematic diagram of the on-chip FM-EYCDWA.

between different modes in FM-EYCDWA, a layer of 400 nm thick $Si_3N_4$ is deposited on top of the erbium–ytterbium co-doped waveguide to complete the eccentric design of the waveguide structure. Moreover, due to the height difference between the passive and active regions, a three-dimensional (3D) taper is designed at the output end of MUX and the input end of DEMUX to ensure a smooth transition between mode fields at different heights.

### A. Hybrid (De)Multiplexer

Many high-performance silicon-on-insulator (SOI)-based devices, such as the mode (DE)MUX [38,39], polarization rotator (PR) [16], and polarization splitter rotator (PSR) [40], have been previously proposed. However, there has been limited attention on comparable devices based on the $Si_3N_4$ platform [41,42], particularly those based on the 800 nm thick $Si_3N_4$ platform, which are not widely reported. To achieve efficient $TE_0$-$TE_0$ coupling, $TE_0$-$TE_1$ mode conversion, $TE_0$-$TM_0$ polarization conversion, and $TM_0$-$TM_1$-$TM_0$ conversion for the 1550 nm band, and also for effective $TE_0$-$TE_0$ coupling and $TE_0$-$TE_1$ mode conversion for the 980 nm band, it is necessary to successfully couple various light modes at 1550 nm and 980 nm into the same bus waveguide. In this context, the phase-matching condition between neighboring waveguides must be satisfied, such that the effective refractive index is equal. Figure 2 illustrates the effective refractive index and waveguide width curves of the strip waveguide based on an 800 nm thick $Si_3N_4$ platform.

To efficiently achieve mode conversion, an asymmetric directional coupler (ADC) structure is utilized in the 1550 nm band to transfer optical power between two adjacent waveguides, as depicted in Fig. 3(a). The sizes of the waveguides

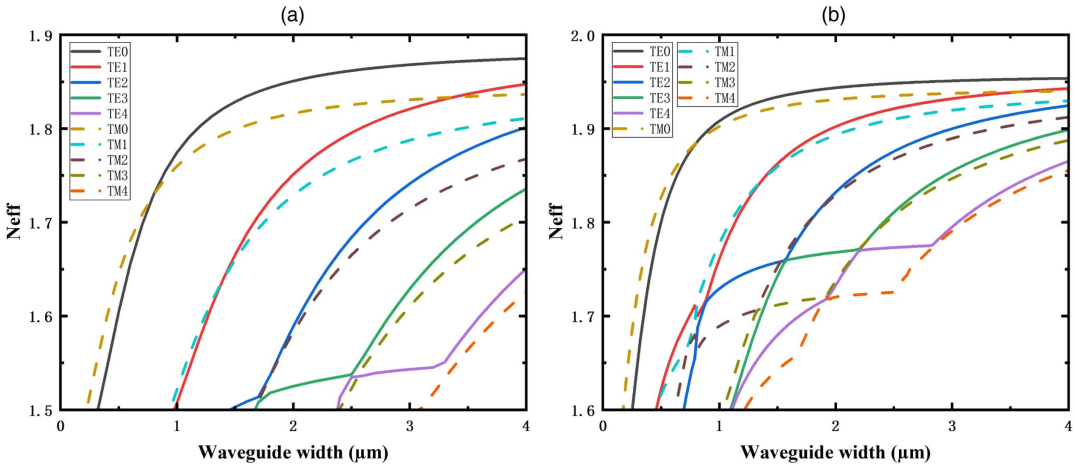


**Fig. 2.** Relationship between waveguide width and effective refractive index at different wavelength. (a) 1550 nm. (b) 980 nm.

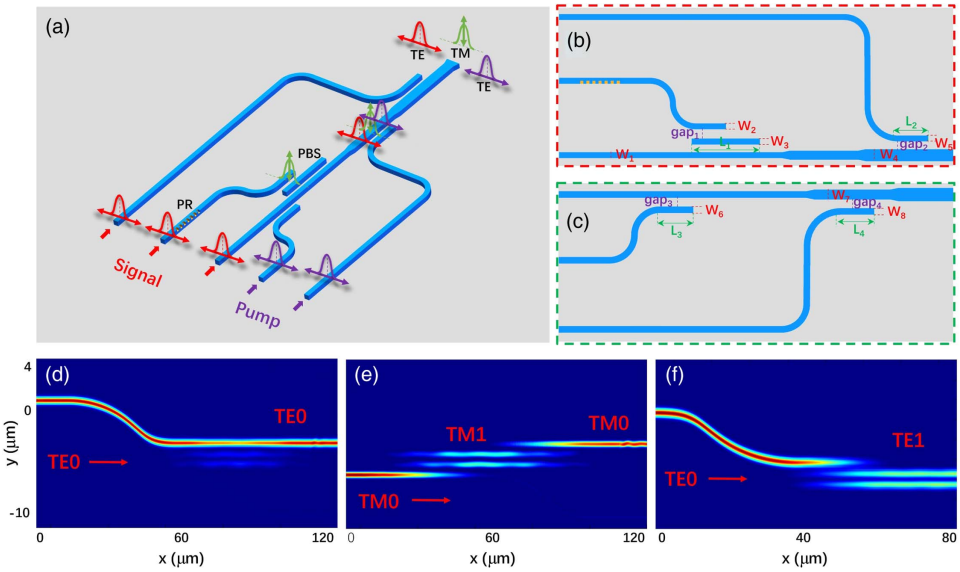


**Fig. 3.** (a) 3D schematic of the proposed MUX, (b) top view of the proposed PBS at the 1550 nm wavelength, and (c) top view of the ADC at the 980 nm wavelength. (d)–(f) Light propagation of (d) $TE_0$-$TE_0$, (e) $TM_0$-$TM_1$-$TM_0$, and (f) $TE_0$-$TE_1$ in the corresponding coupler at 1550 nm wavelength.

are crucial in determining the efficiency of the coupling. Initially, a PBS was designed to allow the entry of the $TE_0$ mode and $TM_0$ mode into the few-mode waveguide. The $TE_0$ mode light is directly output from the few-mode waveguide since it does not satisfy the mode matching requirement. Unlike the $TE_0$ mode, $TM_0$ mode light can enter the few-mode waveguide through cross coupling as it meets the mode matching condition, and it will transition to $TM_1$ mode in the middle wide waveguide. Figure 3(b) illustrates that the waveguides in the coupling region are set apart by a gap, with a width of $gap_1 = 0.35$ μm. The single-mode waveguide widths are set to be identical, that is, $W_1 = W_2 = 0.8$ μm, and the height of the waveguides is also 0.8 μm. The width of the middle wide waveguide, $W_3$, is 2.05 μm, and the coupling length $L_1$ is set to be 86 μm for optimal conversion efficiency. For $TE_0$-$TE_1$ conversion, the widths of the single-mode waveguide ($W_5$) and bus waveguide ($W_4$) are 0.8 μm and 1.85 μm, respectively. The coupling length $L_2 = 19.06$ μm, and the gap width $gap_2 = 0.4$ μm after optimization. Figures 3(d)–3(f) present simulation diagrams illustrating the optical field transmission from single-mode waveguides to the bus waveguide. Figure 3(d) depicts $TE_0$-$TE_0$ coupling with a coupling efficiency of 98.5%, while Fig. 3(e) displays the conversion of $TM_0$-$TM_1$-$TM_0$ with a conversion efficiency of 88.3%, and Fig. 3(f) shows the conversion of $TE_0$-$TE_1$ with a conversion efficiency of 95.0%.

Achieving polarization conversion from $TE_0$ mode to $TM_0$ mode in thick $Si_3N_4$ platforms is challenging due to the lower refractive index of $Si_3N_4$ compared to silicon. Our proposed design addresses this challenge by utilizing a cut-cornered grating structure that incorporates subwavelength gratings (SWGs). The SWGs create asymmetry in the vertical direction, enabling efficient and broadband polarization conversion. The gratings excite two orthogonal mixed guided modes on an asymmetric cross section when $TE_0$ mode light is input. As they propagate, these modes accumulate phase discrepancies due to beat formation and differing propagation constants. Under ideal conditions, the polarization state rotates 90°, converting from $TE_0$ to $TM_0$ when the propagation length exceeds half a beat and the cumulative phase difference reaches $\pi$. For a high performance, we carefully selected parameters, including a grating period ($\Lambda_1$) of 200 nm, duty cycle ($f_1$) of 0.4, SWG etching width of ($W_{etch}$) 400 nm, SWG etching height ($H_{etch}$) of 340 nm, and a total PR length of 56 μm. These choices have led to a impressive polarization conversion efficiency of 91.0% accompanied by low insertion loss (IL) and crosstalk (CT). In Fig. 4, the simulation diagrams illustrate the optical field transmission from $TE_0$ mode to $TM_0$ mode. It is notable that the $TE_0$ mode (see Ex field) exhibits nearly complete conversion to $TM_0$ mode (see Hx field). The calculated IL and CT of (DE)MUX are shown in Fig. 5 using the 3D-FDTD method. The simulated spectrum indicates that within the wavelength range of 1500–1600 nm, the $TE_0$-$TE_0$ coupling, $TE_0$-$TE_1$ conversion, and $TE_0$-$TM_0$ polarization conversion exhibit extremely low IL (<0.6 dB). Moreover, the $TM_0$-$TM_1$-$TM_0$ mode conversion demonstrates a low IL below 1.2 dB within the same wavelength range. Additionally, the crosstalk resulting from $TE_0$-$TE_1$ and $TE_0$-$TM_0$ conversion is below −30 dB and −15 dB, respectively, within the wavelength range of 1500–1600 nm.

In the 980 nm band, we employed a similar structure to achieve $TE_0$-$TE_0$ mode coupling and $TE_0$-$TE_1$ mode conversion, as depicted in Fig. 3(c). The 980 nm single-mode waveguide ($W_6$) was set to a width of 0.8 μm for $TE_0$-$TE_0$ coupling, with a coupling length $L_3$ of 20 μm and a gap width ($gap_3$) of 0.1 μm between the two waveguides. Furthermore, for $TE_0$-$TE_1$ conversion, we adjusted the width of the coupled bus waveguide ($W_7$) to 1.745 μm, with a coupling length ($L_4$) of 19.5 μm and a 0.1 μm gap ($gap_4$) between the bus waveguide and the single-mode waveguide. Figure 6 shows the simulation diagram of optical field transmission. It depicts the $TE_0$-$TE_0$ coupling in Fig. 6(a), with an impressive coupling efficiency of 99.0%, and the mode conversion of $TE_0$-$TE_1$ in Fig. 6(b), with a conversion efficiency of 95.1%. The calculated IL and CT of (DE)MUX at wavelengths ranging from 930 nm to 1030 nm are presented in Fig. 7. It is evident that the $TE_0$-$TE_0$ coupling exhibits low IL (<0.75 dB), and the $TE_0$-$TE_1$ conversion demonstrates low IL (<1.2 dB) and CT (< −25 dB).

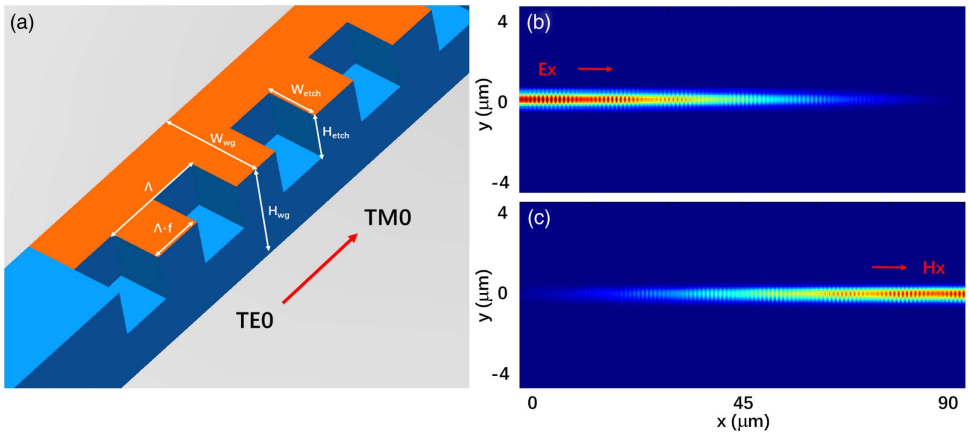


**Fig. 4.** (a) 3D schematic of the proposed PR. (b), (c) Light propagation profiles for the PR at 1550 nm wavelength for (b) $TE_0$ mode and (c) $TM_0$ mode.

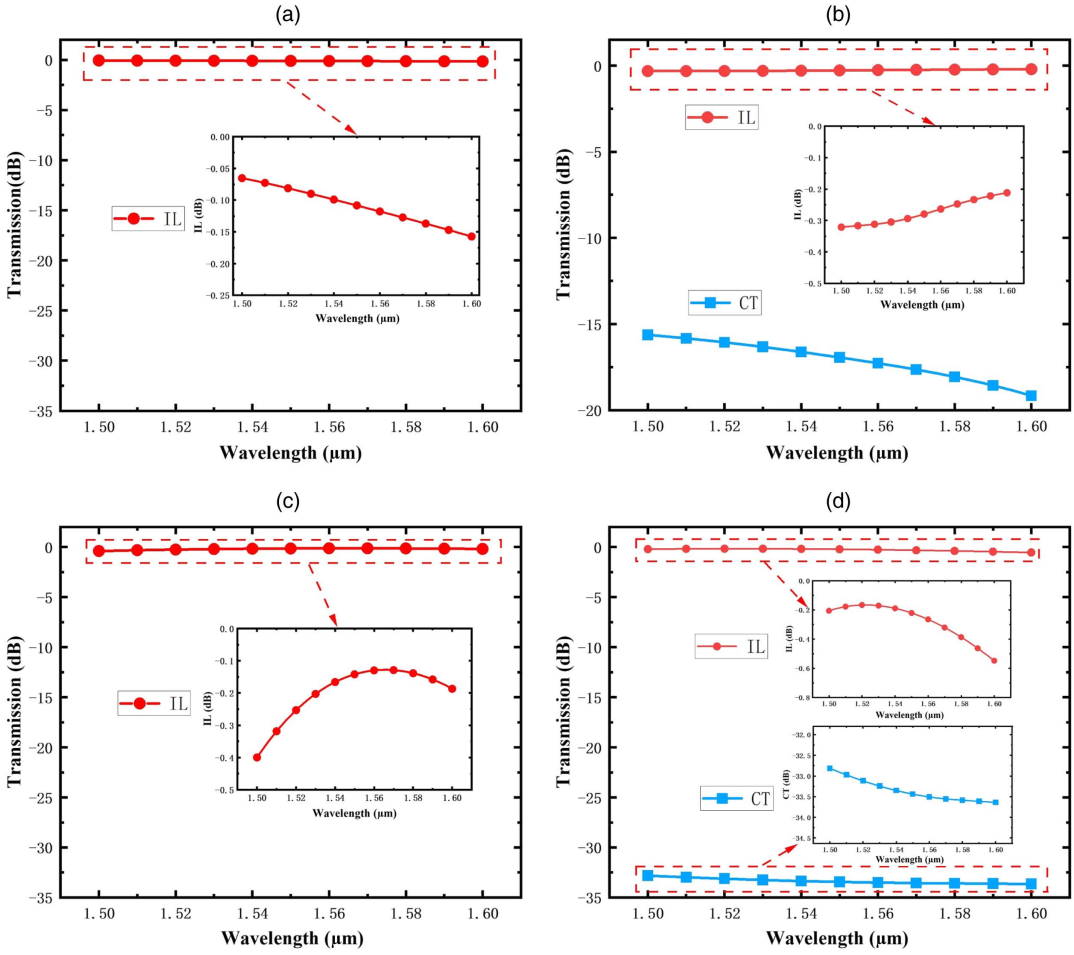


**Fig. 5.** Calculated IL and CT at wavelengths from 1500 nm to 1600 nm. (a) $TE_0$-$TE_0$, (b) $TE_0$-$TM_0$, (c) $TM_0$-$TM_1$-$TM_0$, and (d) $TE_0$-$TE_1$.

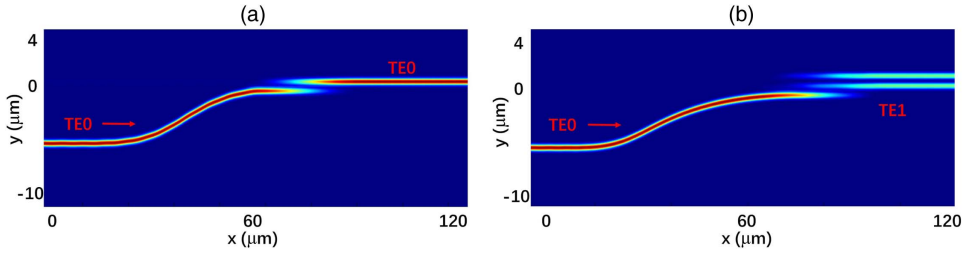


**Fig. 6.** Light propagation of (a) $TE_0$-$TE_0$ and (b) $TE_0$-$TE_1$ in the corresponding coupler at 980 nm wavelength.

### B. Eccentric Structure of Erbium–Ytterbium Co-Doped Waveguide

Using uniform doping, adjusting the pumping scheme is a common approach to achieve a balanced gain, mitigating unequal gain among different modes in FM-EYCDWA. However, the gain of the $TE_0$ mode is prone to loss, limiting the equalization effect of this method. The possibility of attaining gain equalization by non-uniform doping was discussed in Zhang's work [28], albeit with some technological difficulties. In order to address this issue, we present a process-achievable eccentric waveguide structure ensuring high gain for each mode and enabling gain equalization between modes under uniform doping. In the eccentric design, an undoped $Si_3N_4$ layer is deposited above the gain layer. The entire optical field is shifted upwards to establish the necessary eccentric design on the gain layer, leveraging the comparable refractive index of $Si_3N_4$ and Er-Yb co-doped material. Furthermore, we designed a 3D taper to ensure a smooth transition of light between the passive and active layers. Grayscale lithography is employed to fabricate the taper.

In Fig. 8, the $TE_0$ mode is illustrated, with $h_1$, $h_2$, and $\Delta h$ denoting the height of the Er-Yb co-doped waveguide, the

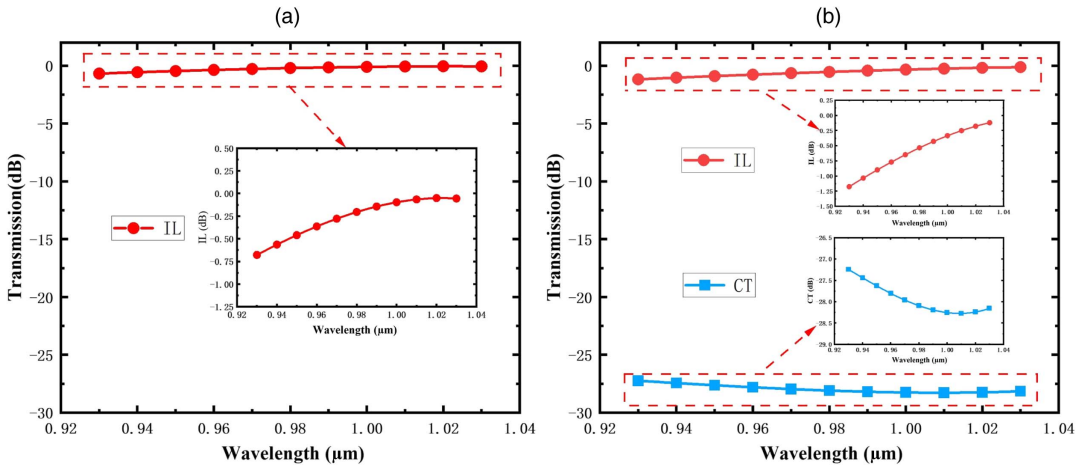


**Fig. 7.** Calculated IL and CT at wavelengths from 930 nm to 1030 nm. (a) $TE_0$-$TE_1$ and (b) $TE_0$-$TM_0$.

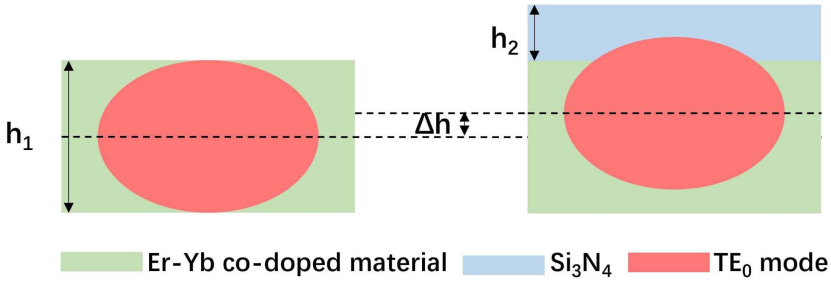


**Fig. 8.** Diagram of the designed eccentric waveguide structure.

thickness of the deposited undoped $Si_3N_4$ layer, and the upward shift distance of the optical field, respectively. At the beginning, the center of the gain layer exhibits the peak light intensity in the vertical direction. Because of the comparable refractive index of the undoped $Si_3N_4$ layer and the Er-Yb co-doped material, the $Si_3N_4$ layer deposited on top of the gain layer using LPCVD causes the vertical expansion of the $TE_0$ mode and an upward shift of the peak intensity by approximately half of $h_2$. As a result, light penetrates the top $Si_3N_4$ layer and the vertical light field distribution in the gain layer becomes asymmetrical. Similar to non-uniform doping techniques, this eccentric structure design balances the DMG between the $TE_0$ mode and other modes by partially mitigating the field confinement factor of the $TE_0$ mode in the gain layer. Instead of adjusting the doping concentration, this eccentric structural design makes it possible to directly manipulate the distribution of the light field within the gain layer, in contrast to intricate non-uniform doping procedures. Furthermore, because it decreases the need to fabricate erbium-doped materials in different concentrations, the eccentric uniform-doping waveguide structure is easier to fabricate than the non-uniform doping coronal configuration.

### C. Fabrication Processes

$Si_3N_4$ has emerged as a favorable process platform for silicon-based optoelectronics due to its low optical loss and compatibility with CMOS processes. The traditional method of preparing waveguides entails growing a uniform layer of $Si_3N_4$ on the substrate and subsequently lithographing the waveguide structure using a mask. However, this method often results in limited thickness of $Si_3N_4$ growth (typically 300–500 nm) due to stress constrains. Ligentec's 800 nm thick $Si_3N_4$ platform, on the other hand, employs the Damascus process. In this process, a thick silicon dioxide BOX layer is first grown on the substrate, and then grooves are etched downwards for depositing $Si_3N_4$. This approach helps alleviate stress distribution across the entire chip and prevents the occurrence of fractures when depositing a thick $Si_3N_4$ layer.

Figure 9 illustrates the preparation processes for FM-EYCDWA. The substrate is divided into three regions: A, B, and C. Regions A and C are used for MUX and DEMUX preparation, respectively, while region B is dedicated to the preparation of Er-Yb co-doped few-mode waveguides. Figures 9(b)–9(d) depict cross-sectional views of the waveguide structure in the *xz* plane. The waveguide shape is etched in $SiO_2$, and an 800 nm thick $Si_3N_4$ layer is deposited through the LPCVD process to complete the preparation of passive devices in regions A and C. Figures 9(e)–9(i) represent cross-sectional views of the waveguide structure in the *yz* plane. In region B, an 800 nm thick Er-Yb co-doped layer is selectively deposited. Atomic layer deposition (ALD) is a powerful technique for selective doping, enabling the direct deposition of

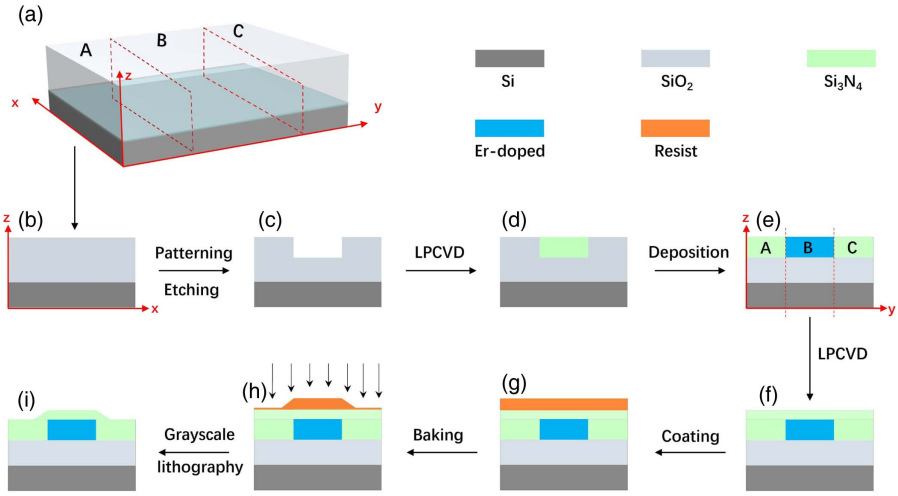


**Fig. 9.** Fabrication processes for an FM-EYCDWA.

gain media onto passive devices to establish the integration between active and passive components [37]. To achieve the eccentric structure design in the active region, a 400 nm thick $Si_3N_4$ layer is deposited atop the Er-Yb co-doped waveguide, and a 3D taper is prepared. Grayscale lithography is a crucial step in the fabrication process of the 3D tapers on the Er-Yb co-doped few-mode waveguides; it utilizes locally adjusted exposure doses to define the 3D structure in the photoresist. Varied exposure doses lead to different depths on the photoresist surface, thereby forming a 3D taper structure with gradual height changes.

## 3. FM-EYCDWA THEORETICAL MODEL

When multiple modes of light propagate concurrently in a few-mode waveguide, the competition between erbium ions in the upper and lower energy levels is an inevitable phenomenon. The combined influences of pump light and signal light lead to the redistribution of erbium ions in the upper and lower energy levels. The conventional theoretical model for gain characteristic in SM-EYCDWA [43] is no longer applicable and requires reanalysis in the context of different modes. Calculating mode field confinement factors suitable for different modes is a critical aspect. In FM-EYCDWA, the modified signal optical mode field confinement factor is defined as follows:

$$\Gamma_i' = \frac{\sum_{j=1}^{N} \Gamma_{ji}^{\text{ions}} P_j^p}{\sum_{j=1}^{N} P_j^p}. \tag{1}$$

In the equation above, $i$ and $j$ represent the mark numbers for the signal and pump modes, and the term $\Gamma_{ji}^{\text{ions}}$ is the normalized overlap integral factor, defined as

$$\Gamma_{ji}^{\text{ions}} = \iint_A \psi_i^s(x,y) g_{\text{ions}}(x,y)\mathrm{d}x\mathrm{d}y \frac{\iint_A \psi_j^p(x,y)\psi_i^s(x,y)\mathrm{d}x\mathrm{d}y}{\sqrt{\iint_A [\psi_j^p(x,y)]^2\mathrm{d}x\mathrm{d}y \iint_A [\psi_i^s(x,y)]^2\mathrm{d}x\mathrm{d}y}}. \tag{2}$$

$\iint_A \psi_i^s(x,y) g_{\text{ions}}(x,y)\mathrm{d}x\mathrm{d}y$ is the traditional definition of the overlap integration factor of signal light, and $g_{\text{ions}}(x,y)$ represents the lateral doping distribution function of the dopant; in the case of uniform doping, $g_{\text{ions}}(x,y) = 1$. Since achieving non-uniform doping in process is challenging, our design employs a waveguide structure based on uniform doping with Er-Yb ions. The concentration of Yb ions is much higher than that of Er ions, and the absorption cross section of Yb ions at 980 nm wavelength is much larger than that of Er ions. The lifetime of the first excited state of Yb ions is much shorter than that of the first excited state of Er ions. In addition, the power of the signal light is significantly lower than that of the pump light; therefore, in the transmission within a few-mode waveguide, the influence of the signal light on the pump light is very small, and the traditional field confinement factor remains applicable in describing the distribution of the pump light in the few-mode waveguide:

$$\Gamma_j^{\text{ions}} = \iint_A \psi_j^p(x,y) g_{\text{ions}}(x,y)\mathrm{d}x\mathrm{d}y. \tag{3}$$

As different signal light modes in the FM-EYCDWA system need to be amplified simultaneously, and considering the shorter lifetime of high excited state energy levels of erbium ions, the number of particles at these levels will rapidly approach zero. To simplify the calculation, we disregard these energy levels and model the population of erbium ions as a two-level system. Our design relies on uniform doping, that is, $g_{\text{ions}}(x,y) = 1$. By incorporating the definition of the modified signal optical mode field confinement factor, the modified rate equations are given by

$$\left[\frac{\sigma_{12}(\nu_s)}{A h\nu_s}\sum_{i=1}^{L}\Gamma_i^{\text{ions}}P_i^s(Z)-\frac{\sigma_{13}(\nu_p)}{A h\nu_p}\sum_{j=1}^{N}\Gamma_j^{\text{ions}}P_j^p(Z)\right]N_1(Z)+\left[\frac{1}{\tau_{21}}+\frac{\sigma_{21}(\nu_s)}{A h\nu_s}\sum_{i=1}^{L}\Gamma_i^{\text{ions}}P_i^s(Z)\right]N_2(Z)+C_2N_2^2(Z)-K_{\text{tr}}N_1(Z)N_2^{\text{Yb}}(Z)=0, \tag{4}$$

$$N_1(Z)+N_2(Z)=N_{\text{Er}}(Z), \tag{5}$$

$$\left[-\frac{\sigma_{12}^{\text{Yb}}(\nu_p)}{A h\nu_p}\sum_{j=1}^{N}\Gamma_j^{\text{ions}}P_j^p(Z)\right]N_1^{\text{Yb}}(Z)+\left[\frac{1}{\tau_{21}^{\text{Yb}}}+\frac{\sigma_{12}^{\text{Yb}}(\nu_p)}{A h\nu_p}\sum_{i=1}^{N}\Gamma_j^{\text{ions}}P_j^p(Z)\right]N_2^{\text{Yb}}(Z)+K_{\text{tr}}N_1(Z)N_2^{\text{Yb}}(Z)=0, \tag{6}$$

$$N_1^{\text{Yb}}(Z)+N_2^{\text{Yb}}(Z)=N_{\text{Yb}}(Z). \tag{7}$$

The rate equations distinguish between SM-EYCDWA and FM-EYCDWA by expanding from the original single signal and pump mode light to multiple modes working together. Likewise, the power transfer equations differ from those of SM-EYCDWA and can be described as follows:

$$\frac{\mathrm{d}P_i^s(Z)}{\mathrm{d}Z}=\Gamma_i'P_i^s(Z)[\sigma_{21}(\nu_s)N_2(Z)-\sigma_{12}(\nu_s)N_1(Z)]-\alpha_i^sP_i^s(Z)-\sum_{l}^{L}d_{il}[P_i^s(Z)-P_l^s(Z)], \tag{8}$$

$$\frac{\mathrm{d}P_j^p(Z)}{\mathrm{d}Z}=-\Gamma_j^{\text{ions}}P_j^p(Z)[\sigma_{13}(\nu_p)N_1(Z)+\sigma_{12}^{\text{Yb}}(\nu_p)N_1^{\text{Yb}}(Z)-\sigma_{21}^{\text{Yb}}(\nu_p)N_2^{\text{Yb}}(Z)]-\alpha_j^pP_j^p(Z)-\sum_{n}^{N}d_{jn}[P_j^p(Z)-P_n^p(Z)]. \tag{9}$$

**Table 1. Parameter Values Used for Modeling**

| Parameter | Symbol | Value |
|---|---|---|
| $Er^{3+}$ concentration | $N_{\text{Er}}$ | $1.644\times10^{27}$ m$^{-3}$ |
| $Yb^{3+}$ concentration | $N_{\text{Yb}}$ | $1.644\times10^{27}$ m$^{-3}$ |
| $Er^{3+}$ absorption cross section at 1530 nm | $\sigma_{12}$ | $5.051\times10^{-25}$ m$^2$ |
| $Er^{3+}$ emission cross section at 1530 nm | $\sigma_{21}$ | $7.303\times10^{-25}$ m$^2$ |
| $Er^{3+}$ absorption cross section at 980 nm | $\sigma_{13}$ | $7.028\times10^{-25}$ m$^2$ |
| $Er^{3+}$ emission cross section at 980 nm | $\sigma_{31}$ | $1.251\times10^{-25}$ m$^2$ |
| $Yb^{3+}$ absorption cross section at 980 nm | $\sigma_{12}^{\text{Yb}}$ | $1.0\times10^{-24}$ m$^2$ |
| $Yb^{3+}$ emission cross section at 980 nm | $\sigma_{21}^{\text{Yb}}$ | $1.0\times10^{-24}$ m$^2$ |
| $Er^{3+}$ lifetime at $^4I_{11/2}$ level | $\tau_{32}$ | 2 μs |
| $Er^{3+}$ lifetime at $^4I_{13/2}$ level | $\tau_{21}$ | 4.23 ms |
| $Yb^{3+}$ lifetime | $\tau_{21}^{\text{Yb}}$ | 1.1 ms |
| Pump wavelength | $\lambda_p$ | 980 nm |
| Signal wavelength | $\lambda_s$ | 1530 nm |
| Propagation loss of the pump laser | $\alpha_p$ | 1 dB/cm |
| Propagation loss of the signal laser | $\alpha_s$ | 1 dB/cm |

In the equations above, $d_{il}$ represents the power coupling coefficient between the $i$th signal mode and the $l$th signal mode, while $d_{jn}$ denotes the coupling coefficient between the $j$th pump mode and the $n$th pump mode. The variables $i$ and $j$ are used as labels for the signal modes and pump modes, respectively, and $L$ and $N$ denote the maximum values of these two variables. Considering the short length of the Er-Yb co-doped waveguide, the influence of the modal coupling effect can be ignored in the simulation.

## 4. GAIN CHARACTERISTICS OF THE FM-EYCDWA

The gain of FM-EYCDWA based on a thick $Si_3N_4$ platform can be calculated using the fourth-order Runge–Kutta method and the theoretical model established in Section 3. The parameters [35] used in the gain characteristics simulation are shown in Table 1.

### A. Without Gain Equalization

Maintaining constant signal and pump power, the gain characteristics of optical waveguide amplifiers are influenced by the length of the optical waveguide device. From Fig. 10(a),

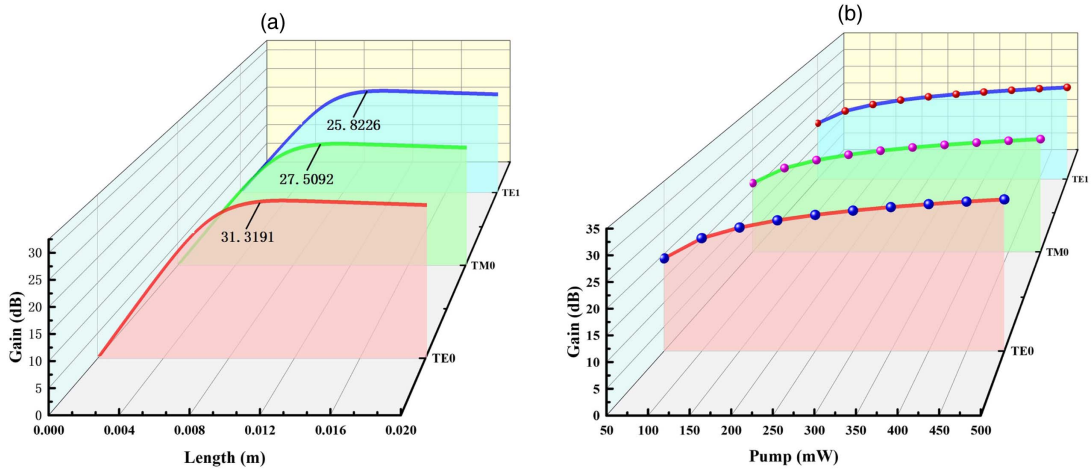


**Fig. 10.** (a) Gain characteristics under different length. (b) Gain characteristics under different pump power.

it is clear that the gain variation trend of the three signal modes in the FM-EYCDWA is consistent. As the waveguide length increases, it can be seen that the gain of the three signal modes increases with the increase of waveguide length, but slightly decreases after reaching a maximum value. This phenomenon reflects that during the transmission process of the pump light in the optical waveguide, in order to generate the inversion of the erbium particles, the energy of the pump light will be absorbed by the particles and continuously consumed. Once the waveguide length hits the optimal value, the device's threshold power surpasses the pump light power, causing the signal light amplification to cease and a slight drop in the device gain from the peak. This is consistent with the performance in SM-EYCDWA. According to the results, the gain of the three modes peaks at a waveguide length of approximately 1.1 cm. When only using the 500 mW $TE_0$ mode pump, the maximum gain in $TE_0$ mode is 31.3 dB, while the gains in $TM_0$ and $TE_1$ modes are 27.5 dB and 25.8 dB, respectively.

For further analysis, we chose the Er-Yb co-doped waveguide with a length of 1.1 cm, at which the waveguide amplification gain is close to saturation. The corresponding parameters are as follows: the signal wavelength is 1550 nm, the pump wavelength is 980 nm, and the initial power of the signal light is 0.1 mW. Figure 10(b) indicates that the gain trend of the signal light in the three modes of FM-EYCDWA remains consistent as the pump power increases. Initially, the signal light's gain rapidly increases with increased pump power. Later on, the gain change is less noticeable, and it stabilizes and approaches saturation. The gain trends of different modes in FM-EYCDWA follow the basic law of SM-EYCDWA. However, if only $TE_0$ mode pumping is used, there is a significant difference of approximately 5.5 dB in different signal optical modes between FM-EYCDWA, necessitating gain equalization.

### B. With Gain Equalization

DMG is mostly caused by the different corrected field confinement factor ($\Gamma_i'$). Equation (1) clearly illustrates that $\Gamma_i'$ is related to the overlap integral factor between the signal light and the pump light as well as the traditional signal field confinement factor. We calculated the overlap integral factors of various signal light modes and pump light modes in the few-mode waveguide to facilitate a more intuitive comparison, as presented in Table 2. The closer the values of the overlap integral factor, the closer the gain of the corresponding modes. Clearly, in the case of using only the $TE_0$ mode pumping scheme, there are differences in the overlap integral factors between $TE_0$ pump mode and three signal modes ($TE_0$, $TM_0$, and $TE_1$), especially the substantial discrepancy (~0.13) between the $TE_0$ signal mode and the $TE_1$ signal mode, resulting in a considerable gain disparity (~5.5 dB) between the $TE_0$ signal mode and $TE_1$ signal mode. Thus, it is imperative to balance the overlap factors to reduce the gain differentials between distinct signal modes. Table 2 demonstrates that there is a significant overlap between the $TE_1$ signal mode and the $TE_1$, $TM_1$ pump modes. Therefore, opting for either of these two pump modes, in conjunction with $TE_0$ pump mode for co-propagating pumping, can lead to some gain equalization; hence, we have selected the $TE_0$ and $TE_1$ pump modes for our plan.

**Table 2. Overlap Integral Factors of Various Signal and Pump Modes**

| | | Pump | | | | |
|---|---|---|---|---|---|---|
| Overlap | Factors | $TE_0$ | $TM_0$ | $TE_1$ | $TM_1$ | $TE_2$ |
| Signal | $TE_0$ | 0.9889 | 0.9928 | 0.8776 | 0.8522 | 0.8773 |
| | $TM_0$ | 0.9603 | 0.9749 | 0.8623 | 0.8484 | 0.8608 |
| | $TE_1$ | 0.8600 | 0.8714 | 0.9817 | 0.9818 | 0.8967 |

After optimizing, we selected a $TE_0$ pump power of 300 mW and a $TE_1$ pump power of 500 mW. As seen in Fig. 11(a), the gain curves for the $TE_0$ and $TE_1$ modes are in close proximity to each other, and have a DMG of roughly 0.3 dB. The overlap factor between the $TE_1$ pump mode and the $TE_1$ signal mode is quite high (0.9817); however, it is only 0.8623 between the $TE_1$ pump mode and the $TM_0$ signal mode, which explains why the gain differences between the $TM_0$ signal modes and $TE_0$, $TE_1$ signal modes are still larger than 3 dB when using $TE_0$-$TE_1$ co-propagation pumping. Consequently, only using the $TE_0$ and $TE_1$ pump mode for co-propagating pumping, the gain disparities among three

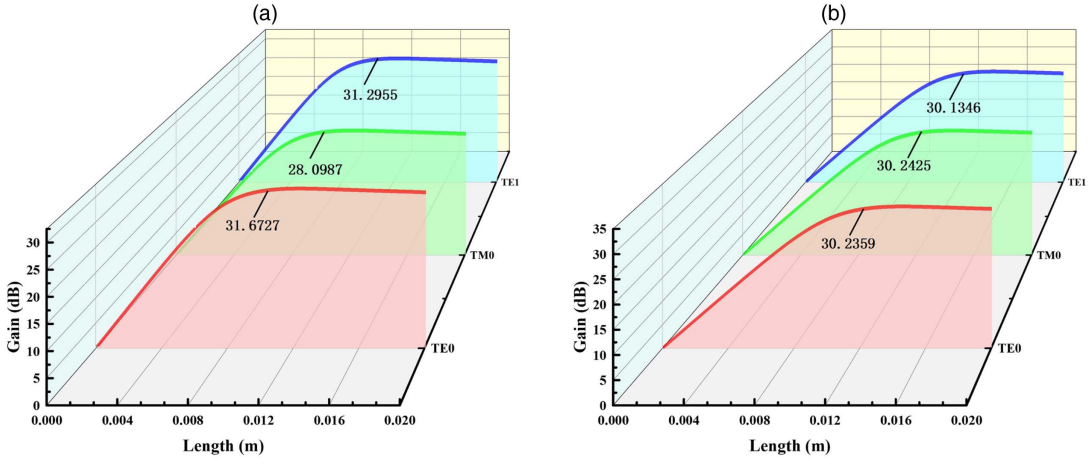


**Fig. 11.** (a) Gain characteristics under co-propagating pumping. (b) Gain characteristics under co-propagating pumping and eccentric design.

**Table 3. Corrected Mode Field Confinement Factors**

| $\Gamma_i'$ | Without DMG Equalization | Co-Propagating Pumping | Co-Propagating Pumping and Eccentric Waveguide Design |
|---|---|---|---|
| $TE_0$ | 0.8846 | 0.8061 | 0.6015 |
| $TM_0$ | 0.7807 | 0.7196 | 0.6016 |
| $TE_1$ | 0.7347 | 0.7981 | 0.5998 |

signal modes ($TE_0$, $TM_0$, and $TE_1$) cannot be balanced simultaneously.

Employing the co-propagating pumping approach, alongside the eccentric structure discussed in Section 2.3, can achieve gain equalization across all signal optical modes in FM-EYCDWA. Table 3 presents the corrected mode field confinement factors ($\Gamma_i'$) before and after DMG equalization. It is evident that without equalization, the differences in $\Gamma_i'$ for the three signal modes are significant. $\Gamma_i'$ between $TE_0$ and $TE_1$ is balanced by using co-propagating pumping method. $\Gamma_i'$ among the three modes of $TE_0$, $TM_0$, and $TE_1$ is balanced when eccentric design is combined with co-propagating pumping. After DMG equalization, the gain and waveguide length curves are depicted in Fig. 11(b). The graph shows that in the FM-EYCDWA, constructed with an eccentric structure, the gain of all the three signal modes surpasses 30 dB, and the DMG is $< 0.1$ dB, providing an effective equalization effect when the input signal light is 0.1 mW, $TE_0$ pump power is 300 mW, and $TE_1$ mode is 500 mW.

## 5. CONCLUSION

In conclusion, to the best of our knowledge, we reported the first on-chip few-mode erbium–ytterbium co-doped waveguide amplifier based on an 800 nm thick $Si_3N_4$ platform, which can achieve high amplification gains and low differential modal gains simultaneously. With the assistance of an eccentric waveguide structure, all three signal modes ($TE_0/TM_0/TE_1$) exhibit amplification gains of more than 30 dB in the case of uniform doping, while maintaining a DMG of less than 0.1 dB. This means that gain equalization in an FM-EYCDWA can be achieved in a more easily implementable way, without losing too much of the gain for each mode. Additionally, the hybrid mode/polarization/wavelength-division (de)multiplexer can be further extended to more channels to accommodate amplification of more modes, indicating its potential for application in integrated MDM systems.

**Funding.** Key Program of the National Natural Science Foundation of China (62035001); Shanghai Science and Technology Innovation Action Plan (22dz208700); International Partnership Program of Chinese Academy of Sciences (18123KYSB20210013).

**Disclosures.** The authors declare no conflicts of interest.

**Data Availability.** Data underlying the results presented in this paper are not publicly available at this time but may be obtained from the authors upon reasonable request.

## REFERENCES

1. R.-J. Essiambre and A. Mecozzi, "Capacity limits in single-mode fiber and scaling for spatial multiplexing," in *Optical Fiber Communication Conference and Exposition/National Fiber Optics Engineers Conference (OFC/NFOEC)* (IEEE, 2012), pp. 1–3.
2. B. Mukherjee, "WDM optical communication networks: progress and challenges," IEEE J. Sel. Areas Commun. **18**, 1810–1824 (2000).
3. D. M. Spirit, A. D. Ellis, and P. E. Barnsley, "Optical time division multiplexing: systems and networks," IEEE Commun. Mag. **32**, 56–62 (1994).
4. D. J. Richardson, J. M. Fini, and L. E. Nelson, "Space-division multiplexing in optical fibres," Nat. Photonics **7**, 354–362 (2013).
5. B. Franz and H. Bülow, "Mode group division multiplexing in graded-index multimode fibers," Bell Labs Tech. J. **18**, 153–172 (2013).
6. Y. Fazea and V. Mezhuyev, "Selective mode excitation techniques for mode-division multiplexing: a critical review," Opt. Fiber Technol. **45**, 280–288 (2018).
7. C. Li, D. Liu, and D. Dai, "Multimode silicon photonics," Nanophotonics **8**, 227–247 (2018).
8. C. Sun, W. Wu, Y. Yu, *et al.*, "De-multiplexing free on-chip low-loss multimode switch enabling reconfigurable inter-mode and inter-path routing," Nanophotonics **7**, 1571–1580 (2018).
9. L.-W. Luo, N. Ophir, C. P. Chen, *et al.*, "WDM-compatible mode-division multiplexing on a silicon chip," Nat. Commun. **5**, 3069 (2014).
10. G.-H. Chen, C.-W. Chow, C.-H. Yeh, *et al.*, "Mode-division-multiplexing (MDM) of 9.4-Tbit/s OFDM signals on silicon-on-insulator (SOI) platform," IEEE Access **7**, 129104–129111 (2019).
11. D. Dai and S. Wang, "Asymmetric directional couplers based on silicon nanophotonic waveguides and applications," Front. Optoelectron. **9**, 450–465 (2016).
12. W. Zhao, Y. Peng, X. Cao, *et al.*, "96-channel on-chip reconfigurable optical add-drop multiplexer for multidimensional multiplexing systems," Nanophotonics **11**, 4299–4313 (2022).
13. H. Shu, B. Shen, Q. Deng, *et al.*, "A design guideline for mode (de)-multiplexer based on integrated tapered asymmetric directional coupler," IEEE Photon. J. **11**, 6603112 (2019).
14. Z. Tao, B. Wang, B. Bai, *et al.*, "An ultra-compact polarization-insensitive slot-strip mode converter," Front. Optoelectron. **15**, 5 (2022).
15. Q. Deng, Q. Yan, L. Liu, *et al.*, "Highly compact polarization insensitive strip-slot waveguide mode converter," in *CLEO: Applications and Technology* (Optica, 2015), paper JTu5A-53.
16. H. Xu and Y. Shi, "Subwavelength-grating-assisted silicon polarization rotator covering all optical communication bands," Opt. Express **27**, 5588–5597 (2019).
17. Q. Huang and K. S. Chiang, "Polarization-insensitive ultra-broadband mode filter based on a 3D graphene structure buried in an optical waveguide," Optica **7**, 744–745 (2020).
18. I. Zegaar, A. Hocini, A. Harhouz, *et al.*, "Design of a double-mode plasmonic wavelength filter using a defective circular nano-disk resonator coupled to two MIM waveguides," Prog. Electromagn. Res. Lett. **104**, 67–75 (2022).
19. M. Salsi, "Challenges of few mode amplifiers," in *Optical Fiber Communication Conference (OFC)* (IEEE, 2014), pp. 1–3.
20. T. Xu, T. Gao, Y. Wang, *et al.*, "High-gain integrated in-line few-mode amplifier enabling 3840-km long-haul transmission," Photon. Res. **10**, 2794–2801 (2022).
21. Y. Liu, Z. Qiu, X. Ji, *et al.*, "A photonic integrated circuit–based erbium-doped amplifier," Science **376**, 1309–1313 (2022).
22. J. Mu, M. Dijkstra, J. Korterik, *et al.*, "High-gain waveguide amplifiers in $Si_3N_4$ technology via double-layer monolithic integration," Photon. Res. **8**, 1634–1641 (2020).
23. J. Rönn, W. Zhang, A. Autere, *et al.*, "Ultra-high on-chip optical gain in erbium-based hybrid slot waveguides," Nat. Commun. **10**, 432 (2019).
24. B. Wang, P. Zhou, X. Wang, *et al.*, "A low-fabrication-temperature, high-gain chip-scale waveguide amplifier," Sci. China Inf. Sci. **65**, 162405 (2022).
25. W. A. Hendriks, L. Chang, C. I. Van Emmerik, *et al.*, "Rare-earth ion doped $Al_2O_3$ for active integrated photonics," Adv. Phys. X **6**, 1833753 (2021).

26. Y. Zhou, Y. Zhu, Z. Fang, *et al.*, "Monolithically integrated active passive waveguide array fabricated on thin film lithium niobate using a single continuous photolithography process," Laser Photon. Rev. **17**, 2200686 (2023).
27. P. Zhou, B. Wang, X. Wang, *et al.*, "Design of an on-chip electrically driven, position-adapted, fully integrated erbium-based waveguide amplifier for silicon photonics," OSA Contin. **4**, 790–814 (2021).
28. X. Zhang, J. Yan, C. Wang, *et al.*, "Design of a few-mode erbium-ytterbium co-doped polymer optical waveguide amplifier with low differential modal gain," J. Lightwave Technol. **39**, 3201–3216 (2021).
29. C. Yu, G. Hu, F. Wang, *et al.*, "Few-mode polymer optical waveguide amplifier for mode-division multiplexed transmission," Opt. Lett. **46**, 5509–5512 (2021).
30. X. Sun, Y. Wang, L. Zhong, *et al.*, "High-order mode waveguide amplifier with high mode extinction ratio written in an $Er^{3+}$-doped phosphate glass," Opt. Express **31**, 5812–5819 (2023).
31. Q. Wilmart, S. Guerber, J. Faugier-Tovar, *et al.*, "A device library for the ultra-low loss $Si_3N_4$ platform," Proc. SPIE **12006**, 120060D (2022).
32. M. A. Gaafar, K. Wang, M. Ludwig, *et al.*, "Photonic-chip integrated large-mode-area high-power CW optical amplifier," EPJ Web Conf. **287**, 01009 (2023).
33. D. B. Bonneville, H. C. Frankis, R. Wang, *et al.*, "Erbium-ytterbium co-doped aluminium oxide waveguide amplifiers fabricated by reactive co-sputtering and wet chemical etching," Opt. Express **28**, 30130–30140 (2020).
34. R. Wang, H. C. Frankis, H. M. Mbonde, *et al.*, "Erbium-ytterbium co-doped aluminum oxide thin films: co-sputtering deposition, photoluminescence, luminescent lifetime, energy transfer and quenching fraction," Opt. Mater. **111**, 110692 (2021).
35. M. Zhang, J. Lu, Y. Chen, *et al.*, "Study on $Er^{3+}$-$Yb^{3+}$ co-doped $La_2O_3$–$Al_2O_3$ glasses for C-band optical waveguide amplifier with high luminous efficiency and low pump threshold," Ceram. Int. **48**, 32236–32240 (2022).
36. Z. Zhang, S. Li, R. Gao, *et al.*, "Erbium-ytterbium codoped thin-film lithium niobate integrated waveguide amplifier with a 27 dB internal net gain," Opt. Lett. **48**, 4344–4347 (2023).
37. A. C. Liapis, V. Pelgrin, P. Liu, *et al.*, "Wafer-scale atomic-layer-deposition of $Er^{3+}$-and $Yb^{3+}$-doped gain materials for integrated photonics," in *Conference on Lasers and Electro-Optics (CLEO)* (IEEE, 2023), pp. 1–2.
38. J. Wang, S. He, and D. Dai, "On-chip silicon 8-channel hybrid (de)multiplexer enabling simultaneous mode-and polarization-division-multiplexing," Laser Photon. Rev. **8**, L18–L22 (2014).
39. Y. He, Y. Zhang, X. Jiang, *et al.*, "On-chip silicon three-mode (de)multiplexer employing subwavelength grating structure," in *European Conference on Optical Communication (ECOC)* (IEEE, 2017), pp. 1–3.
40. J. Chen and J. Xiao, "Ultracompact silicon-based polarization splitter and rotator based on asymmetric directional couplers with subwavelength gratings," J. Opt. Soc. Am. B **39**, 345–354 (2022).
41. Y.-D. Yang, Y. Li, Y.-Z. Huang, *et al.*, "Silicon nitride three-mode division multiplexing and wavelength-division multiplexing using asymmetrical directional couplers and microring resonators," Opt. Express **22**, 22172–22183 (2014).
42. X. Han, Y. Jiang, A. Frigg, *et al.*, "Mode and polarization-division multiplexing based on silicon nitride loaded lithium niobate on insulator platform," Laser Photon. Rev. **16**, 2100529 (2022).
43. Z. Dong, Y. Zhao, Y. Wang, *et al.*, "Gain optimization of an erbium-ytterbium co-doped amplifier via a $Si_3N_4$ photonic platform," Opt. Express **31**, 35419–35430 (2023).